8. L. Rustad, *Nature* **413**, 578 (2001).
9. W. T. Peterjohn, J. M. Melillo, F. P. Bowles, P. A. Steudler, *Oecologia* **93**, 18 (1993).
10. W. T. Peterjohn, J. M. Melillo, P. A. Steudler, K. M. Newkirk, *Ecol. Appl.* **4**, 617 (1994).
11. CO_2 flux measurements were made by placing chamber lids over anchored collars for 15 min and sampling the headspace at 5-min intervals. Samples were analyzed for trace gas concentrations by gas chromatography or infrared analysis, and the changes in concentration were used to calculate net flux rates. On each sampling date, fluxes were measured at early morning and afternoon intervals.
12. J. Grace, M. Rayment, *Nature* **404**, 819 (2000).
13. E. A. Davidson, S. E. Trumbore, R. Amundson, *Nature* **408**, 789 (2000).
14. Net nitrogen mineralization was measured for the organic horizon and upper 10 cm of mineral soil using in situ buried bag incubations. Incubations were for 6 weeks at a time, from April through November, and for 4 months during the winter. Initial samples were collected and analyzed for extractable NH_4^+ and NO_3^- content (extraction with 2N KCl for 48 hours and analysis with standard autoanalyzer methods). The same analysis was carried out on the incubated samples. The difference in total mineral N content between initial and incubated soils is the net mineralization rate. Soil nitrogen was assessed through sampling of organic and mineral soils in all plots in 1992 and again in 1999. Samples were analyzed for carbon and nitrogen content with a Perkin-Elmer CHN analyzer. Concentrations of inorganic nitrogen in water leaching below the rooting zone were measured with high-tension lysimetry. Soil water samples were collected from one porous cup lysimeter per plot on two occasions every month for the first 2 years of the experiment, then once monthly. Lysimeters were placed at a depth of 50 cm and evacuated to 15 inches of mercury for 24 hours before sampling. Samples were frozen until they were analyzed for NH_4^+ and NO_3^-. Nitrous oxide fluxes were measured along with CO_2, with the same static chamber method, from 1991 through 1995. Samples were analyzed for trace gas concentrations by gas chromatography, and the changes in concentration were used to calculate net flux rates.
15. During 1996, we analyzed the lysimeter water samples for dissolved organic nitrogen (DON). We found very low levels of DON in lysimeters from all treatments with no clear treatment differences. DON was estimated as the difference between total dissolved nitrogen (TDN) and dissolved inorganic nitrogen, where TDN was measured by high-temperature platinum–catalyzed combustion (*23*).
16. A. H. Magill *et al.*, *Ecosystems* **3**, 238 (2000).
17. This additional carbon storage in woody tissue was calculated as the product of 12.7% of the cumulative increase in net nitrogen mineralization over the decade (41 g of nitrogen m^{-2}) and the measured carbon:nitrogen mass ratio of the wood (300:1) as follows: 0.127×4 g of nitrogen $m^{-2} \times 300$.
18. This conclusion is based on a paired Student's *t* test with aggregated data from the six experimental blocks.
19. J. Bergh, S. Linder, T. Lundmark, B. Elfving, *For. Ecol. Manage.* **119**, 51 (1999).
20. P. Jarvis, S. Linder, *Nature* **405**, 904 (2000).
21. J. Harte *et al. Ecol. Appl.* **5**, 132 (1995).
22. Y. Luo, S. Wan, S. Hui, L. Wallace, *Nature* **413**, 622 (2001).
23. J. Merriam, W. H. McDowell, W. S. Currie, *Soil Sci. Soc. Am. J.* **60**, 1050 (1996).
24. Supported by the Office of Science, Biological and Environmental Research Program, U.S. Department of Energy, through the Northeast Regional Center of the National Institute for Global Environmental Change under cooperative agreement no. DE-FC03-90ER61010; NSF's Long-Term Ecological Research Program (contract no. NSF-DEB 0080592); the U.S. Environmental Protection Agency's Global Change Program (contract no. EPA-CR 823713-01-0); and the ExxonMobil Corporation.

20 May 2002; accepted 7 November 2002

Shape-Controlled Synthesis of Gold and Silver Nanoparticles

Yugang Sun and Younan Xia*

Monodisperse samples of silver nanocubes were synthesized in large quantities by reducing silver nitrate with ethylene glycol in the presence of poly(vinyl pyrrolidone) (PVP). These cubes were single crystals and were characterized by a slightly truncated shape bounded by {100}, {110}, and {111} facets. The presence of PVP and its molar ratio (in terms of repeating unit) relative to silver nitrate both played important roles in determining the geometric shape and size of the product. The silver cubes could serve as sacrificial templates to generate single-crystalline nanoboxes of gold: hollow polyhedra bounded by six {100} and eight {111} facets. Controlling the size, shape, and structure of metal nanoparticles is technologically important because of the strong correlation between these parameters and optical, electrical, and catalytic properties.

Metal nanoparticles play important roles in many different areas. For example, they can serve as a model system to experimentally probe the effects of quantum confinement on electronic, magnetic, and other related properties (*1*–*3*). They have also been widely exploited for use in photography (*4*), catalysis (*5*), biological labeling (*6*), photonics (*7*), optoelectronics (*8*), information storage (*9*), surface-enhanced Raman scattering (SERS) (*10*, *11*), and formulation of magnetic ferrofluids (*12*). The intrinsic properties of a metal nanoparticle are mainly determined by its size, shape, composition, crystallinity, and structure (solid versus hollow). In principle, one could control any one of these parameters to fine-tune the properties of this nanoparticle.

Department of Chemistry, University of Washington, Seattle, WA 98195–1700, USA.

*To whom correspondence should be addressed. E-mail: xia@chem.washington.edu

Many metals can now be processed into monodisperse nanoparticles with controllable composition and structure (*13*) and sometimes can be produced in large quantities through solution-phase methods (*14*, *15*). Despite this, the challenge of synthetically controlling the shape of metal nanoparticles has been met with limited success. On the nanometer scale, metals (most of them are face-centered cubic, or fcc) tend to nucleate and grow into twinned and multiply twinned particles (MTPs) with their surfaces bounded by the lowest-energy {111} facets (*16*). Other morphologies with less stable facets have only been kinetically achieved by adding chemical capping reagents to the synthetic systems (*17*–*22*). Here we describe a solution-phase route to the large-scale synthesis of silver nanocubes. Uniform gold nanoboxes with a truncated cubic shape were also generated by reacting the silver cubes with an aqueous $HAuCl_4$ solution.

The primary reaction involved the reduction of silver nitrate with ethylene glycol at 160°C. In this so-called polyol process (*23*), the ethylene glycol served as both reductant and solvent. We recently demonstrated that this reaction could yield bicrystalline silver nanowires in the presence of a capping reagent such as poly(vinyl pyrrolidone) (PVP) (*24*). Subsequent experiments suggested that the morphology of the product had a strong dependence on the reaction conditions. When the concentration of $AgNO_3$ was increased by a factor of 3 and the molar ratio between the repeating unit of PVP and $AgNO_3$ was kept at 1.5, single-crystalline nanocubes of silver were obtained (*25*). Figure 1, A and B, show scanning electron microscope (SEM) images of a typical sample of silver nanocubes and indicate the large quantity and good uniformity that were achieved using this approach. These silver nanocubes had a mean edge length of 175 nm, with a standard deviation of 13 nm. Their surfaces were smooth, and some of them self-assembled into ordered two-dimensional (2D) arrays on the silicon substrate when the SEM sample was prepared. It is also clear from Fig. 1B that all corners and edges of these nanocubes were slightly truncated. Figure 1C shows the transmission electron microscope (TEM) image of an array of silver nanocubes self-assembled on the surface of a TEM grid. The inset shows the electron diffraction pattern obtained by directing the electron beam perpendicular to one of the square faces of a cube. The square symmetry of this pattern indicates that each silver nanocube was a single crystal bounded mainly by {100} facets. On the basis of these SEM and TEM studies, it is clear that the slightly truncated nanocube could be described by the drawing shown in

Fig. 1D. The x-ray diffraction (XRD) pattern recorded from the same batch of sample (supported on a silicon substrate as in Fig. 1A) is also displayed in Fig. 1D, and the peaks were assigned to diffraction from the (111), (200), and (220) planes of fcc silver, respectively. The lattice constant calculated from this pattern was 4.088 Å, a value in agreement with the literature report (a = 4.086 Å, Joint Committee on Powder Diffraction Standards file no. 04-0783). It is worth noting that the ratio between the intensities of the (200) and (111) diffraction peaks was higher than the conventional value (0.67 versus 0.4), indicating that our nanocubes were abundant in {100} facets, and thus their {100} planes tended to be preferentially oriented (or textured) parallel to the surface of the supporting substrate (*26*). The ratio between the intensities of the (220) and (111) peaks was also slightly higher than the conventional value (0.33 versus 0.25) because of the relative abundance of {110} facets on the surfaces of our silver nanocubes.

The morphology and dimensions of the product were found to strongly depend on reaction conditions such as temperature, the concentration of $AgNO_3$, and the molar ratio between the repeating unit of PVP and $AgNO_3$. For example, when the temperature was reduced to 120°C or increased to 190°C, the product was dominated by nanoparticles with irregular shapes. The initial concentration of $AgNO_3$ had to be higher than ~0.1 M, otherwise silver nanowires were the major product. If the molar ratio between the repeating unit of PVP and $AgNO_3$ was increased from 1.5 to 3, MTPs became the major product. Silver nanocubes of various dimensions could be obtained by controlling the growth time (*25*). Figure 2, A and B, show TEM images for 17- and 14-min growth times, and the nanocubes had a mean edge length of 115 ± 9 and 95 ± 7 nm, respectively. Figure 2C shows a TEM image of the sample that was synthesized using a lower concentration (0.125 M) of $AgNO_3$ and a shorter growth time (30 min). The mean edge length of these silver nanocubes decreased to 80 ± 7 nm. Silver nanocubes with smaller sizes (~50 nm, Fig. 2D) have also been obtained at a shorter growth time (25 min), although some of these particles have not been able to evolve into complete cubes. These demonstrations suggest that it is possible to tune the size of silver nanocubes by controlling the experimental conditions.

As illustrated by Wang (*27*), the shape of an fcc nanocrystal was mainly determined by the ratio (R) between the growth rates along <100> and <111> directions. Octahedra and tetrahedra bounded by the most stable {111} planes will be formed when R = 1.73, and perfect cubes bounded by the less stable {100} planes will result if R is reduced to 0.58. For the slightly truncated nanocubes illustrated in Fig. 1D, the ratio R should have a value close to 0.7. If PVP was not present, the silver atoms generated by reducing silver nitrate with ethylene glycol nucleated and grew into MTPs bounded by the most stable {111} facets (*28*). When PVP was introduced, it is believed that the selective interaction between PVP and various crystallographic planes of fcc silver could greatly reduce the growth rate along the <100> direction and/or enhance the growth rate

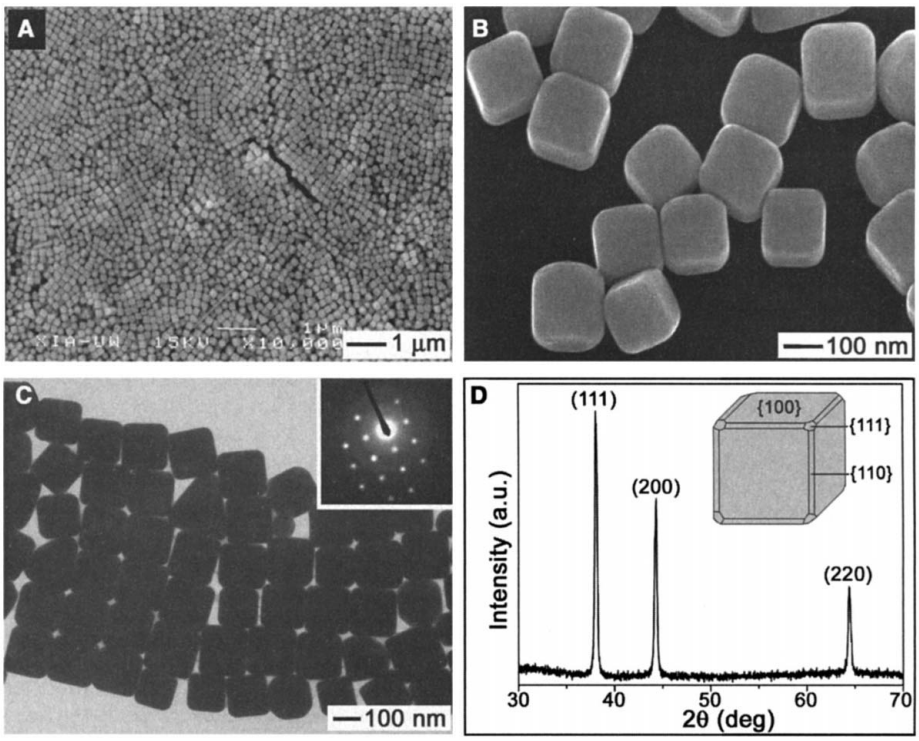

Fig. 1. (**A**) Low- and (**B**) high-magnification SEM images of slightly truncated silver nanocubes synthesized with the polyol process. The image shown in (**B**) was taken at a tilting angle of 20°. (**C**) A TEM image of the same batch of silver nanocubes. The inset shows the diffraction pattern recorded by aligning the electron beam perpendicular to one of the square faces of an individual cube. (**D**) An XRD pattern of the same batch of sample, confirming the formation of pure fcc silver. a.u., arbitrary units.

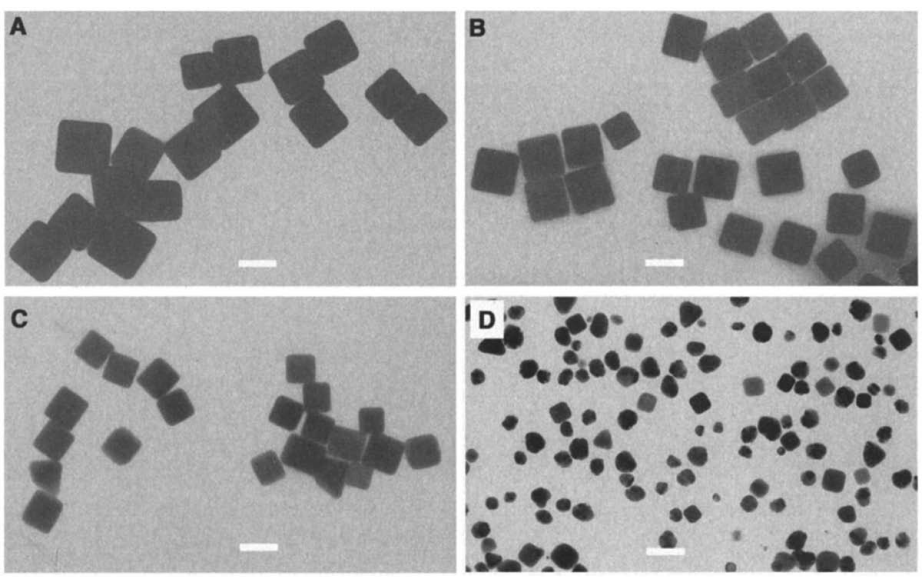

Fig. 2. TEM images of silver nanocubes synthesized under different conditions. (**A** and **B**) The same as in Fig. 1, except that the growth time was shortened from 45 min to 17 and 14 min, respectively. (**C** and **D**) The same as in Fig. 1, except that the $AgNO_3$ concentration was reduced from 0.25 to 0.125 M and the growth time was shortened to 30 and 25 min, respectively. Scale bars, 100 nm.

along the <111> direction, and thus reduce R from 1.73 to 0.7. Both Fourier transform infrared and x-ray photoelectron spectroscopy measurements indicate that there exists a strong interaction between the surfaces of silver nanoparticles and PVP through coordination bonding with the O and N atoms of the pyrollidone ring (*29*, *30*), although the exact bonding geometry and the nature of selectivity between different crystallographic planes are still not clear.

We have also exploited the use of these silver nanocubes as sacrificial templates to generate gold nanoboxes with a well-defined shape and hollow structure (*31*–*33*)

$$3Ag(s) + HAuCl_4(aq) \rightarrow Au(s) + 3AgCl(aq) + HCl(aq) \quad (1)$$

Based on this stoichiometric relationship, it was possible to completely convert silver nanocubes into soluble species and thus leave behind a pure solid product in the form of gold nanoboxes (*34*). Figure 3A shows an SEM image of silver nanocubes after they had reacted with an insufficient amount of $HAuCl_4$, as calculated from Eq. 1. The black spots represent pinholes in their surfaces, where no gold had been deposited through the replacement reaction. It is believed that the existence of such pinholes allowed for the transport of chemical species into and out of the gold boxes until the reaction had been completed. The locations of these black spots implied that the replacement reaction occurred on the surface of a template in the following order: {110}, {100}, and {111} facets. This sequence was consistent with the order of free energies associated with these crystallographic planes: $\gamma_{\{110\}} > \gamma_{\{100\}} > \gamma_{\{111\}}$ (*27*).

The gold nanoboxes shown in Fig. 3B self-assembled into a close-packed 2D array during sample preparation. The size of these gold boxes increased by ~20% as compared with that of the silver templates. Such an increase in size was in agreement with the shell thickness calculated from stoichiometric and geometric arguments. The gold nanoboxes were finished with smooth surfaces, and most of them (>95%) were free of defects such as pinholes. Each box was bounded by two sets of facets (eight triangular facets and six square ones), and any one of these facets could lie against a solid substrate. The inset of Fig. 3B shows the SEM image of an individual box sitting on a silicon substrate against one of its triangular facets, illustrating the high symmetry of this polyhedral hollow nanoparticle. The crystallinity and structure of these gold nanoboxes were examined using electron diffraction. Figure 3, C and D, show the electron diffraction patterns obtained from two gold nanoboxes sitting on the TEM grids against one of their square and triangular faces, respectively. These diffraction spots suggest that each nanobox was a single crystal, with its square facets being indexed to {100} planes and triangular ones to {111} planes. On the basis of these observations, we believe that an epitaxial relationship might exist between the surfaces of the silver cubes and those of the gold boxes that greatly facilitated the transformation from the single-crystalline templates to the single-crystalline products. Minor reconstruction also occurred in the replacement process; for example, the {110} planes that were observed as ridges on the surfaces of silver cubes disappeared, and the areas of {111} and {100} facets were enlarged and reduced, respectively.

Silver nanocubes with controllable dimensions were synthesized by means of a modified polyol process that involved the reduction of silver nitrate with ethylene glycol in the presence of a capping reagent such as PVP. Although the fundamental basis of shape selectivity for this system has yet to be fully understood, it is believed that the selective adsorption of PVP on various crystallographic planes of silver played the major role in determining the product morphology. Uniform gold nanoboxes having a highly truncated cubic shape were also synthesized by reacting the silver nanocubes with an aqueous $HAuCl_4$ solution. These silver and gold nanoparticles should find use in a variety of areas that include photonics, catalysis, and SERS-based sensing. This work and previous demonstrations from other groups (*17*–*22*) make it clear that chemical synthesis of metal nanoparticles with well-controlled shapes, sizes, and structures is a practical reality. The major requirement seems to be the selection of a capping reagent that is able to chemically modify various faces of a metal with an appropriate selectivity.

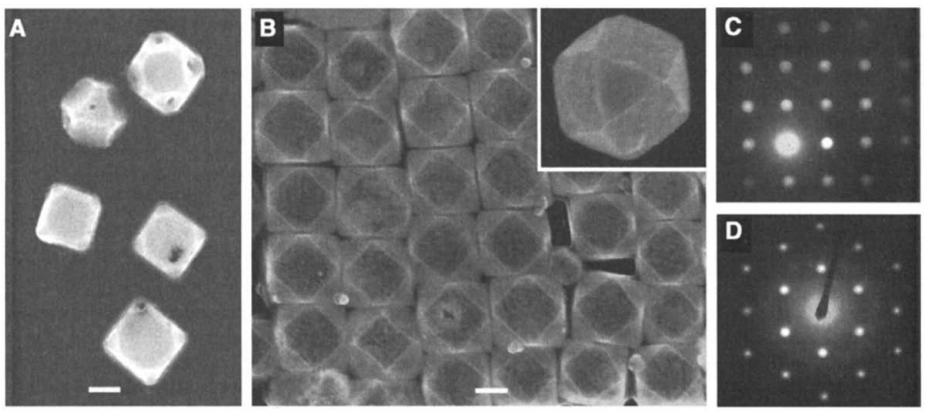

Fig. 3. SEM images of silver nanocubes (Fig. 1) after they had reacted with **(A)** 0.3 ml and **(B)** 1.5 ml of aqueous $HAuCl_4$ solution (1 mM). As indicated by the black spots in (A), the {111} facets of gold nanoboxes were incompletely closed in the early stages of this replacement reaction, when $HAuCl_4$ was in deficiency (as calculated from the stoichiometric equation). If excess $HAuCl_4$ solution was added [as in (B)], the area of {111} facets could increase up to a maximum value at the expense of {100} and {110} facets. **(C** and **D)** Electron diffraction patterns of two gold nanoboxes with their square and triangular facets oriented perpendicular to the electron beam, respectively. Scale bars, 100 nm.

References and Notes

1. W. P. Halperin, *Rev. Mod. Phys.* **58**, 533 (1986).
2. A. C. Templeton, W. P. Wuelfing, R. W. Murray, *Acc. Chem. Res.* **33**, 27 (2000).
3. M. A. El-Sayed, *Acc. Chem. Res.* **34**, 257 (2001).
4. D. M.-K. Lam, B. W. Rossiter, *Sci. Am.* **265**, 80 (May 1991).
5. L. N. Lewis, *Chem. Rev.* **93**, 2693 (1993).
6. S. R. Nicewarner-Peña *et al.*, *Science* **294**, 137 (2001).
7. S. A. Maier *et al.*, *Adv. Mater.* **13**, 1501 (2001).
8. P. V. Kamat, *J. Phys. Chem. B* **106**, 7729 (2002).
9. C. B. Murray, S. Sun, H. Doyle, T. Betley, *Mater. Res. Soc. Bull.* **26**, 985 (2001).
10. S. Nie, S. R. Emory, *Science* **275**, 1102 (1997).
11. L. A. Dick, A. D. McFarland, C. L. Haynes, R. P. Van Duyne, *J. Phys. Chem. B* **106**, 853 (2002).
12. M.-P. Pileni, *Adv. Funct. Mater.* **11**, 323 (2001).
13. H. Bönnemann, J. Hormes, U. Kreibig, in *Handbook of Surface and Interfaces of Materials*, H. S. Nalwa, Ed. (Academic Press, San Diego, CA, 2001), pp. 1–87.
14. G. Schmid, *Chem. Rev.* **92**, 1709 (1992).
15. D. V. Goia, E. Matijevic, *New J. Chem.* **22**, 1203 (1998).
16. J. G. Allpress, J. V. Sanders, *Surf. Sci.* **7**, 1 (1967).
17. A. I. Kirkland *et al.*, *Proc. R. Soc. London Ser. A* **440**, 589 (1993).
18. T. S. Ahmadi, Z. L. Wang, T. C. Green, A. Henglein, M. A. El-Sayed, *Science* **272**, 1924 (1996).
19. J. S. Bradley, B. Tesche, W. Busser, M. Maase, M. T. Reetz, *J. Am. Chem. Soc.* **122**, 4631 (2000).
20. V. F. Puntes, K. M. Krishnan, A. P. Alivisatos, *Science* **291**, 2115 (2001).
21. N. Cordente *et al.*, *Nano Lett.* **1**, 565 (2001).
22. R. Jin *et al.*, *Science* **294**, 1901 (2001).
23. F. Fievet, J. P. Lagier, M. Figlarz, *Mater. Res. Soc. Bull.* **14**, 29 (December 1989).
24. Y. Sun, Y. Xia, *Adv. Mater.* **14**, 833 (2002).
25. In a typical synthesis of silver nanocubes, 5 ml of anhydrous ethylene glycol (Aldrich, 99.8%) was heated at 160°C for 1 hour. 3 ml of ethylene glycol solution of $AgNO_3$ (0.25 M, Aldrich, 99+%) and 3 ml of ethylene glycol solution of PVP (0.375 M in repeating unit, weight-average molecular weight ≈ 55,000, Aldrich) were simultaneously added to the ethylene glycol by means of a two-channel syringe pump at a rate of 0.375 ml/min. The reaction mixture was then continued with heating at 160°C for another 45 min. The product was dominated by cubic nanoparticles, with a small amount (<5%) of silver nanowires. These nanowires could easily be separated from nanocubes through filtration because of their large difference in dimension. In this case, the reac-

tion mixture was diluted with water (25 times by volume) and filtered through Nucleopore membranes (Whatman, Clifton, NJ) that contained pores 1 μm in diameter. The silver nanocubes could be recovered from ethylene glycol through centrifugation and then redispersed into water.
26. B. D. Cullity, S. R. Stock, *Elements of X-Ray Diffraction* (Prentice-Hall, Upper Saddle River, NJ, ed. 3, 2001), pp. 402–404.
27. Z. L. Wang, *J. Phys. Chem. B* **104**, 1153 (2000).
28. C. Ducamp-Sanguesa, R. Herrera-Urbina, M. Figlarz, *J. Solid State Chem.* **100**, 272 (1992).
29. Z. Zhang, B. Zhao, L. Hu, *J. Solid State Chem.* **121**, 105 (1996).
30. F. Bonet, K. Tekaia-Elhsissen, K. V. Sarathy, *Bull. Mater. Sci.* **23**, 165 (2000).
31. S. J. Oldenburg, R. D. Averitt, S. L. Westcott, N. J. Halas, *Chem. Phys. Lett.* **288**, 243 (1998).
32. W. Lin, T. H. Warren, R. G. Nuzzo, G. S. Girolami, *J. Am. Chem. Soc.* **115**, 11644 (1993).
33. Y. Sun, B. T. Mayers, Y. Xia, *Nano Lett.* **2**, 481 (2002).
34. In a typical procedure for the preparation of gold nanoboxes, a 5-ml aliquot of the aqueous dispersion containing silver nanocubes was refluxed for 10 min. Aliquots of 1 mM $HAuCl_4$ (99.9%, Aldrich) aqueous solution were added dropwise to the refluxing solution. This mixture was continuously refluxed until its color became stable. Vigorous magnetic stirring was maintained throughout the synthesis.
35. Supported in part by the Office of Naval Research (grant N-00014-01-1-0976), a Career Award from NSF (grant DMR-9983893), and a research fellowship from the David and Lucile Packard Foundation. Y.X. is a Camille Dreyfus Teacher Scholar (2002–2007) and an Alfred P. Sloan Research Fellow (2000–2002). We thank D. Qin of the Nanotech User Facility for SEM analysis and X. Jiang, Y. Yin, Y. Lu, B. Mayers, and T. Herricks for their help with electron and x-ray diffraction studies.

12 August 2002; accepted 6 November 2002

Observation of a Strongly Interacting Degenerate Fermi Gas of Atoms

K. M. O'Hara, S. L. Hemmer, M. E. Gehm, S. R. Granade, J. E. Thomas*

We report on the observation of a highly degenerate, strongly interacting Fermi gas of atoms. Fermionic lithium-6 atoms in an optical trap are evaporatively cooled to degeneracy using a magnetic field to induce strong, resonant interactions. Upon abruptly releasing the cloud from the trap, the gas is observed to expand rapidly in the transverse direction while remaining nearly stationary in the axial direction. We interpret the expansion dynamics in terms of collisionless superfluid and collisional hydrodynamics. For the data taken at the longest evaporation times, we find that collisional hydrodynamics does not provide a satisfactory explanation, whereas superfluidity is plausible.

As the fundamental constituents of matter are interacting fermions, the experimental study of strongly interacting, degenerate Fermi gases will have an impact on theories in fields from particle physics to materials science. Although the interactions between fermions are understood when they are weak (e.g., quantum electrodynamics), the treatment of very strong interactions requires the development of new theoretical approaches. Testing these new approaches requires experimental systems with widely tunable interaction strengths, densities, and temperatures. Ultracold atomic Fermi gases have exactly these properties, and thus enable tests of calculational techniques for fundamental systems ranging from quarks in nuclear matter to electrons in high-temperature superconductors (*1–11*). For this reason, a number of groups are developing methods for creating and exploring ultracold atomic Fermi gases (*12–17*). We report on the study of a strongly interacting, degenerate Fermi gas. In contrast to the isotropic expansion previously observed for a noninteracting degenerate Fermi gas (*12*), we observe anisotropic expansion when the gas is released from an optical trap.

An exciting feature of strongly interacting atomic Fermi gases is the possibility of high-temperature superfluids that are analogs of very high temperature superconductors (*8–11*). Our experiments produce the conditions predicted for this type of superfluid transition. Further, the anisotropic expansion we observe has been suggested as a signature of the onset of superfluidity in a Fermi gas (*18*). We interpret the observed anisotropic expansion in terms of both collisionless superfluid hydrodynamics (*18*) and a new form of collisional hydrodynamics.

Strong, magnetically tunable interactions are achieved in our experiments by using a Fermi gas comprising a 50-50 mixture of the two lowest hyperfine states of ^{6}Li, i.e., the $|F = ½, M = ±½\rangle$ states in the low magnetic field basis. This mixture has a predicted broad Feshbach resonance near an applied magnetic field of 860 G (*19, 20*), where the energy of a bound ^{6}Li-^{6}Li molecular state is tuned into coincidence with the total energy of the colliding atoms. This enables the interaction strength to be widely varied (*19–22*). It has also been suggested that interactions between fermions can be modified by immersion in a Bose gas (*23*). Our experiments are performed at 910 G, where the zero-energy scattering length a_S is estimated to be $\sim -10^4\ a_0$ ($a_0 = 0.53 \times 10^{-8}$ cm) and the gas has strongly attractive interactions. Resonance superfluidity has been predicted to occur at this magnetic field for sufficiently low temperatures (*11*).

In our experiments, ^{6}Li atoms are loaded from a magneto-optical trap into an ultrastable CO_2 laser trap (*15*). The trap oscillation frequencies are $\omega_z = 2\pi \times (230 \pm 20$ Hz) for the axial (z) direction and $\omega_\perp = 2\pi \times (6625 \pm 50$ Hz) for the transverse direction. Rate equation pumping is used to produce the 50-50 spin mixture: A broadband radio frequency (rf) field centered at 7.4 MHz is applied at a magnetic field of ~8 G, nulling the population difference according to $\Delta n(t) = \Delta n(0)\ \exp(-2Rt)$, where R is the pumping rate. In our experiments, $2R = 600\ s^{-1}$; applying the rf field for $t = 0.1$ s produces precise population balance.

We achieve very low temperatures via rapid forced evaporation in the CO_2 laser trap. In contrast to experiments that use magnetic traps to achieve degeneracy (*12–14, 16, 17*), this approach has several natural advantages. First, we are able to evaporate both spin states to degeneracy at the desired magnetic field of 910 G. As a result, the sample is never exposed to fields near 650 G where loss and heating are observed (*19, 24*). Second, the evaporation process is identical for both spin states, thereby maintaining the initial spin balance as well as Fermi surface matching. Third, at this field, the collision cross section is extremely large and unitarity-limited, so that runaway evaporation is expected (*25*).

Forced evaporation is achieved by lowering the power of the trapping laser while maintaining the beam profile and angular alignment. The trap depth U is reduced for 3.5 s according to the trajectory $U(t) = U_0(1 + t/\tau)^{-1.45} + U_B$ (*25*), where U_B is a small offset. The value of τ is taken to be 0.1 s, large compared to the time constant estimated for achieving degeneracy at 910 G. With this choice, very high evaporation efficiency is achieved, yielding extremely low temperatures.

After evaporation, the trap is adiabatically recompressed to full depth over 0.5 s and then held for 0.5 s to ensure thermal equilibrium. While maintaining the applied magnetic field of 910 G, the gas is released from the trap and imaged at various times to observe the anisotropy. The CO_2 laser power is extinguished in less than 1 μs with a rejection ratio of 2×10^{-5} (*15*).

Physics Department, Duke University, Durham, NC 27708, USA.

*To whom correspondence should be addressed. E-mail: jet@phy.duke.edu